Frontiers of Optoelectronics (2026) 19:23
https://doi.org/10.2738/foe.2026.0023

Frontiers of Optoelectronics

RESEARCH ARTICLE

Outage analysis and optimization for IRS-UAV-assisted FSO systems under malicious jamming

Jingyu Wang[1,2] · Dingshan Gao (✉)[1] · Juan Li[2] · Xinliang Zhang[1] · Deqiang Ding[2]

Abstract

This paper proposes a robust design for a free-space optical (FSO) system assisted by an unmanned aerial vehicle (UAV) equipped with an intelligent reflecting surface (IRS), operating under probabilistic malicious jamming. The UAV-carried IRS establishes an auxiliary link when the direct path is blocked. The system experiences composite fading (saturated turbulence, pointing errors, and angle-of-arrival fluctuations), and the jammer's intermittent activity is modeled by a Bernoulli process. We derive a closed-form expression for the average outage probability (OP) under this unified channel-and-jamming model. To address the critical performance-cost trade-off, a bi-objective optimization problem is formulated to jointly minimize the OP and the hardware deployment cost. An alternating optimization (AO) algorithm is proposed to solve the resulting mixed-integer nonlinear programming problem by decoupling it into discrete (number of IRS elements) and continuous (power, angles, apertures) subproblems, which are efficiently handled via integer search and particle swarm optimization, respectively. Simulation results demonstrate that the proposed AO algorithm converges within 15 iterations, substantially faster than genetic algorithm and random search, and achieves a near-optimal trade-off, reducing outage probability by an order of magnitude compared to non-optimized benchmarks while keeping hardware cost within budget.

Keywords Intelligent reflecting surface · Free-space optical communication · Malicious jamming · Outage probability · Alternating optimization

1 Introduction

The integration of unmanned aerial vehicles (UAVs) and free-space optical (FSO) communications has emerged as a promising paradigm for enabling high-capacity and flexible wireless networks [1]. However, FSO links are highly susceptible to atmospheric turbulence (AT), pointing errors (PE), and blockages due to their strict dependence on line-of-sight (LoS) conditions [2]. Intelligent reflecting surfaces (IRSs) have garnered significant attention in recent years as a cost-effective solution for reconfiguring propagation environments [3]. When mounted on UAVs, IRSs can establish virtual LoS links, thereby enhancing the coverage and robustness of FSO communications [4]. Nevertheless, UAV mobility introduces uncertainties in IRS positioning and orientation, leading to additional angle-of-arrival (AoA) fluctuations and exacerbated PE [5,6]. Moreover, FSO channels are inherently vulnerable to malicious jamming attacks, particularly from UAV-mounted jammers capable of executing adaptive strategies [7].

Prior work has characterized outage performance in IRS-assisted FSO systems under various impairments [8–10], yet important limitations persist. Recent studies have examined related problems, but none has jointly addressed the specific challenges tackled here. Table 1 compares this study with recent representative contributions along four lines, namely, inclusion of UAV-enabled jamming, the composite channel model adopted, formulation of a perfor-

✉ Dingshan Gao
dsgao@mail.hust.edu.cn

Jingyu Wang
wangjingyu@nudt.edu.cn

Juan Li
lijuan17a@nudt.edu.cn

Xinliang Zhang
xlzhang@mail.hust.edu.cn

Deqiang Ding
dingdeqiang@nudt.edu.cn

[1] Wuhan National Laboratory for Optoelectronics, Huazhong University of Science and Technology, Wuhan 430074, China

[2] School of Optical Communication, Engineering University of Information Support Force, PLA, Wuhan 430035, China

Table 1 Comparison of related works on IRS-UAV-assisted FSO systems under jamming.

Reference	UAV jamming	Composite channel model	Bi-objective optimization	AO algorithm
Saxena and Chung [13]	✓	Gamma-Gamma + PE	×	×
Sharma and Swaminathan [14]	×	IGGG Turb. + PE + AoA	×	×
Wang et al. [15]	✓	Gamma-Gamma + PE	×	×
Wang et al. [16]	✓	Gamma-Gamma + PE + AoA	×	×
Singh et al. [17]	✓	Path loss	×	×
Gu and Mohajer [4]	×	Path loss	✓	×
Vishwakarma et al. [10]	×	Turbulence + PE	×	×
Xu et al. [11]	×	Gamma-Gamma + Málaga + PE + AoA	×	×
Qu et al. [12]	×	Shadowed Rician + Málaga + PE	×	×
This work	✓	**Saturated Turb. + PE + AoA + Bernoulli jamming**	✓	✓

mance-cost bi-objective optimization problem, and development of a low-complexity alternating optimization algorithm.

UAV-assisted FSO relaying has also attracted considerable attention. Xu et al. [11] developed a unified analysis of dual-hop FSO/FSO systems with amplify-and-forward (AF) relaying, accounting for attenuation, atmospheric turbulence, pointing errors, and angle-of-arrival (AOA) fluctuations. Qu et al. [12] extended this line of work to space-air-ground integrated networks (SAGIN), analyzing asymmetric RF/FSO hybrid relay links under shadowed Rician fading and Málaga turbulence. Both works, however, concentrate on active relay architectures and limit their analysis to normal (unjammed) operating conditions. They do not account for malicious jamming, a critical concern for military and secure communications, nor do they tackle the practical trade-off between performance and deployment cost that motivates our work.

Motivated by the need to characterize malicious jamming threats, Saxena and Chung [13] analyzed jamming effects in IRS-assisted UAV dual-hop FSO systems, but their model assumes constant jamming and does not address system-level optimization. Sharma and Swaminathan [14] provided a comprehensive performance analysis of UAV-based IRS-assisted FSO systems incorporating AoA fluctuations, though their work does not account for jamming threats. Wang et al. [15] recently presented an IRS-assisted multi-link FSO system under UAV-enabled jamming; however, they employ a Gamma-Gamma turbulence model suited primarily to weak-to-moderate regimes and do not formulate an optimization problem. Another recent study [16] investigates UAV-assisted jamming in IRS-enhanced FSO systems with Gamma-Gamma turbulence, deriving closed-form expressions for outage probability, average bit error rate, and ergodic capacity. It, too, assumes constant jamming and omits cost-aware optimization. Singh et al. [17] formulated a mirror element allocation problem to mitigate reactive jamming in optical IRS and UAV-assisted FSO networks, representing an important step toward optimization-based anti-jamming design. Their work, however, centers on resource allocation for multi-user quality-of-service satisfaction rather than the physical-layer performance-cost trade-off under composite channel impairments. Gu and Mohajer [4] investigated multi-IRS-empowered UAV communications for throughput maximization, and Vishwakarma et al. [10] studied cascaded FSO systems with optical reflecting surfaces; neither considers jamming.

This paper differs from prior work in three respects. First, we adopt a unified composite channel model that integrates saturated (negative-exponential) turbulence, more appropriate for the strong turbulence regime typical of low-altitude UAV FSO links, with pointing errors and AoA fluctuations. Second, we employ a probabilistic Bernoulli jamming model that captures the intermittent "attack-idle" duty cycle characteristic of battery-constrained UAV jammers. Third, we formulate a bi-objective optimization framework that explicitly balances outage performance against hardware deployment cost, solved via a tailored alternating optimization algorithm of low computational complexity. To our knowledge, no prior work has addressed these three aspects jointly within a unified analytical and optimization framework.

To bridge these gaps, the core contributions of this paper are summarized as follows:

(1) We propose an IRS-UAV-assisted FSO system model under probabilistic jamming, characterized by a Bernoulli random process. This formulation captures the intermittent attack pattern as a fundamental threat model, a notable departure from the constant jamming assumption preval-

ent in the literature. We integrate this model with a composite channel description that unifies saturated (negative-exponential) turbulence, PE, and AoA fluctuations for the cascaded IRS link, and derive a novel closed-form expression for the average outage probability (OP).

(2) We formulate a bi-objective optimization problem that jointly minimizes the system OP and the total hardware cost (which scales with the number of IRS elements, N). This formulation explicitly addresses the critical performance–cost trade-off essential for practical, resource-constrained UAV-IRS deployments.

(3) We develop a customized hybrid alternating optimization (AO) algorithm that exploits the problem's inherently decomposable structure. The algorithm decouples the mixed-integer nonlinear programming problem into discrete (number of IRS elements) and continuous (transmit power, optical angles, aperture sizes) subproblems, which are efficiently handled via integer search and particle swarm optimization, respectively. The proposed algorithm achieves near-optimal performance with low computational complexity, rendering it suitable for real-time UAV applications.

(4) Through extensive numerical simulations, we provide clear engineering insights into parameter sensitivities (e.g., the relative importance of hardening the IRS-D link versus the S-IRS link under jamming, and the optimal trade-off between field-of-view and aperture size). We also benchmark the proposed AO algorithm against standard metaheuristics to demonstrate its efficacy and convergence advantages.

The remainder of this paper is organized as follows. Section 2 describes the system and channel models. Section 3 presents the outage probability analysis. Section 4 formulates the bi-objective optimization problem and details the proposed alternating optimization algorithm. Section 5 discusses the numerical results, and Section 6 concludes the paper.

2 System and channel model

2.1 System model

As depicted in Fig. 1, we consider an IRS-UAV-assisted FSO communication system under UAV-enabled malicious jamming. The direct LoS link between the source (S) and destination (D) is blocked. A UAV-carried IRS is deployed to establish an auxiliary cascaded S-IRS-D FSO link. The IRS comprises N reflecting elements, each capable of independently adjusting the phase shift of the incident optical signal. A malicious jammer (J) launches adaptive optical jamming attacks towards D with a certain probability. The received signal y_s at D from the s-th reflecting element of the IRS can be expressed as

$$y_s = R\sqrt{P_s}h_s\upsilon_s + R\sqrt{P_j}h_j\Lambda\upsilon_j + n_s, \tag{1}$$

where $R = 1$ A/W is the photodetector responsivity [7], $\upsilon_s \in \{0,1\}$ is the modulated OOK symbol, $\upsilon_j \equiv 1$ denotes

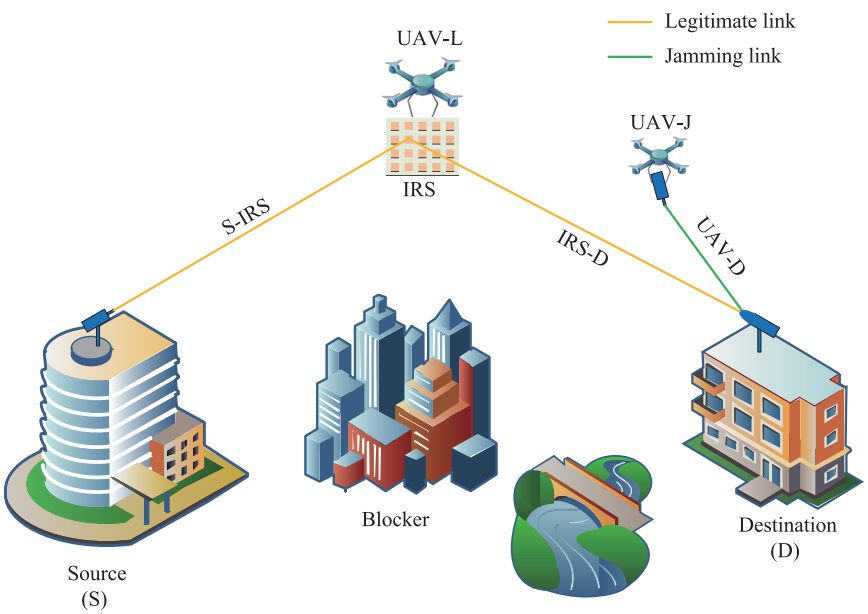

Fig. 1 Schematic of an IRS-UAV-assisted FSO system countering UAV-enabled malicious jamming.

continuous-wave optical jamming signal, and $n_s \sim \mathcal{N}(0,\sigma^2)$ is the additive white Gaussian noise (AWGN). P_s and P_j are the transmit powers of the legitimate signal and the jamming signal, respectively. The channel gains of the cascaded S-IRS-D link and the jamming link are denoted by h_s and h_j, respectively.

The jamming state Λ is modeled as a Bernoulli random variable: $\Pr(\Lambda = 1) = \rho$ (jamming active), and $\Pr(\Lambda = 0) = 1-\rho$ (jamming idle), where ρ is the jamming probability and the jamming power is set to

$$P_j = \frac{\bar{P}_j}{\rho}, \qquad \bar{P}_j : \text{average jamming power.} \tag{2}$$

The Bernoulli jamming model is appropriate for this work for three key reasons. First, it faithfully represents the intermittent operation of battery-limited UAV jammers [7,13]. Second, our core analytical and optimization contributions are independent of the specific jamming temporal structure; more complex models would preclude closed-form derivations. Third, it yields a conservative performance bound under the average power constraint $\bar{P}_j$, guaranteeing that our anti-jamming design is robust to more advanced jamming strategies.

Under the presence of a strong jamming signal ($\Lambda = 1$), the influence of AWGN becomes negligible compared to the jamming [13]. Therefore, the instantaneous electrical signal-to-jamming-plus-noise ratio (SJNR) can be approximated as

$$\gamma_j = \frac{P_s\left(\sum_{s=1}^{N} h_s\right)^2}{\frac{\bar{P}_j h_j^2}{\rho} + \sigma^2} \approx \frac{\rho\bar{\gamma}_j\left(\sum_{s=1}^{N} h_s\right)^2}{h_j^2}, \tag{3}$$

where $\bar{\gamma}_j \triangleq P_s/\bar{P}_j$ represents the average signal-to-jamming ratio (SJR).

The instantaneous electrical SJNR at D depends on the jamming state Λ. We assume the IRS is configured to perform coherent beamforming towards D by optimizing the phase shifts $\{\psi_s\}$. Under this ideal beamforming condition, the effective channel gain for the legitimate signal is $\left|\sum_{s=1}^{N} h_s\right|^2 = N^2h^2$, where we assume i.i.d. channel coefficients h_s for analytical tractability, with h representing the average channel gain per element. Therefore, the electrical SJR can be expressed as

$$\gamma_j = \frac{\rho\bar{\gamma}_j N^2 h^2}{h_j^2}. \tag{4}$$

2.2 Channel model

As shown in Fig. 1, the legitimate S-D channel consists of two cascaded sub-channels: S-IRS and IRS-D, with h_p and h_q denoting their respective channel gains. Following the IRS-assisted channel model in Ref. [2], the end-to-end channel gain is expressed as

$$h_s = h_p \partial e^{j\psi_s} h_q, \tag{5}$$

where ∂ and ψ_s correspond to the amplitude reflection coefficient and induced phase shift of the IRS element at position P. Both the legitimate sub-channels ($\{h_x\}$, $x \in \{p,q\}$) and the jamming channel ($\{h_j\}$) incorporate path loss, AT, PE, and AoA fluctuations induced by UAV jitter.

The combined channel gain h_x can be modeled as

$$h_x = h_{l,x} h_{a,x} h_{p,x} h_{\mathrm{AoA},x}, \quad x \in \{p,q,j\}, \tag{6}$$

where $h_{\mathrm{AoA},x}$ models the AoA fluctuation due to UAV jitter; $h_{l,x} = e^{-\varepsilon L_x}$ is the path loss,with the attenuation coefficient $\varepsilon = \frac{3.91}{V}\left(\frac{\lambda}{550}\right)^{-Q}\mathrm{m}^{-1}$, where V is the visibility, λ is the wavelength in (nm), and Q is the particle size coefficient, and L_x is the link distance. The AT component $h_{a,x}$ follows a negative exponential distribution, $f_{h_{a,x}}(u) = e^{-u}$, modeling saturated AT. $h_{p,x}$ models the PE effect, whose statistics depend on the beam waist and receiver aperture [2]. The probability density function (PDF) of $h_{p,x}$ is given by [2]

$$f_{h_{p,x}}(h_{p,x}) = \frac{\xi_x^2}{A_{0,x}^{\xi_x^2}} h_{p,x}^{\xi_x^2-1}, \qquad 0 \leqslant h_{p,x} \leqslant A_{0,x}, \tag{7}$$

where $A_{0,x} = [\mathrm{erf}(v_x)]^2$ represents the maximum fraction of optical power captured at the IRS and D; $v_x = \frac{a_x\sqrt{\frac{\pi}{2}}}{\omega_{z,x}}$, where a_x is the radius of the receiving aperture, and $\omega_{z,x}$ is the beam waist radius; $\xi_x = \frac{\omega_{\mathrm{zeq},x}}{2\sigma_x}$, where σ_x is the PE displacement standard deviation (jitter) at the receiver.

The equivalent beam width $\omega_{\mathrm{zeq},p}$ at the IRS [7] is expressed as

$$\omega_{\mathrm{zeq},p}^2 = \frac{L_p^3\theta_p\cos^{3/2}(\theta_p/2)\cdot\mathrm{erf}\left(\frac{2a_p\sqrt{\pi\cos(\varphi_p+\theta_p/2)}}{L_p\theta_p\sqrt{2\cos(\theta_p/2)}}\right)}{8\sqrt{2}a_p\cos^{3/2}(\varphi_p+\theta_p/2)\exp\left(-\frac{2\pi a_p^2\cos(\varphi_p+\theta_p/2)}{L_p^2\theta_p^2\cos(\theta_p/2)}\right)}. \tag{8}$$

The equivalent beam width $\omega_{\mathrm{zeq},q}$ at D [7] is expressed as

$$\omega_{zeq,q}^2 = \frac{L_p^3\theta_p\left(\frac{\omega_p+1}{\omega_p}\right)^3\cos^{3/2}(\theta_p/2)}{8\sqrt{2}a_q\cos^{3/2}\left(\varphi_q+\theta_p/2\right)}\times \frac{\operatorname{erf}\left(\frac{2a_q\sqrt{\pi\cos(\varphi_q+\theta_p/2)}}{L_p\theta_p\left(\frac{\omega_p+1}{\omega_p}\right)\sqrt{2\cos(\theta_p/2)}}\right)}{\exp\left(-\frac{2\pi a_q^2\cos(\varphi_p+\theta_p/2)}{L_p^2\theta_p^2\left(\frac{\omega_p+1}{\omega_p}\right)^2\cos(\theta_p/2)}\right)}, \tag{9}$$

where $\omega_p = \frac{L_p}{L_q}$ defines the ratio of the two distance parameters, L_p and L_q correspond to the S-IRS and IRS-D, respectively; θ_p denotes the beam-divergence angle at the IRS, φ_p represents the incident angle at the IRS, and φ_q is the incident angle at D as shown in Fig. 2.

Considering the combined effects of these impairments, the PDF of the composite channel gain h_x is derived in closed-form as [13]

$$f_{h_x}(h_x) = \exp\left(-\frac{\varphi_{\text{AoA}}^2}{2\sigma_{\text{AoA}}^2}\right)\delta(h_x) + \left[1-\exp\left(-\frac{\varphi_{\text{AoA}}^2}{2\sigma_{\text{AoA}}^2}\right)\right] \times \frac{\xi_x^2}{A_{0,x}h_{l,x}}G_{1,2}^{2,0}\left(\frac{h_x}{A_{0,x}}\middle|\begin{matrix}1+\xi_x^2\\ \xi_x^2,\,1\end{matrix}\right), \tag{10}$$

where φ_{AoA} is set to the FoV angle [9] and σ_{AoA} is the standard deviation of the UAV's orientation.

The PDF of the s-th legitimate channel gain h_s is consequently derived as

$$f_{h_s}(t) = \exp\left(-\frac{\varphi_{\text{AoA}}^2}{\sigma_{\text{AoA}}^2}\right)\delta(t) + \left[1-\exp\left(-\frac{\varphi_{\text{AoA}}^2}{2\sigma_{\text{AoA}}^2}\right)\right]^2\frac{\xi_q^2}{A_{0,q}h_{l,q}} \times \frac{\xi_p^2}{A_{0,p}h_{l,p}}G_{2,4}^{4,0}\left(\frac{t}{A_{0,p}A_{0,q}}\middle|\begin{matrix}1+\xi_q^2,\,1+\xi_p^2\\ \xi_p^2,\,1,\,\xi_q^2,\,1\end{matrix}\right). \tag{11}$$

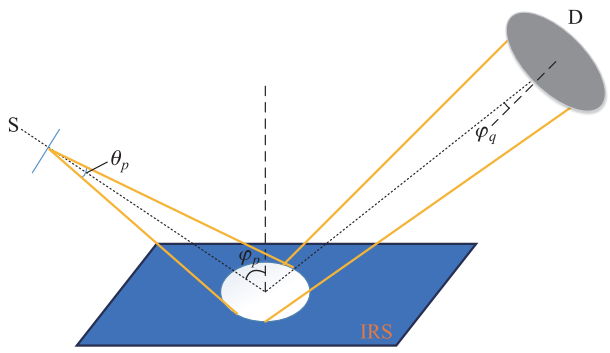

Fig. 2 Beam divergence at IRS.

From Eq. (4), the PDF of γ_j can be expressed as

$$f_{\gamma_j}(\gamma) = \frac{1}{4\sqrt{c\gamma}}\int_0^\infty f_{h_s}(c\gamma y)\,f_{h_j}(y)\,\mathrm{d}y, \tag{12}$$

where $c = \rho\bar{\gamma}_j N^2$.

Substituting Eqs. (10) and (11) into Eq. (12) and applying the integral identity for the Meijer G-function (07.34.21.0011.01) [18], the PDF of γ_j can be derived as

$$f_{\gamma_j}(\gamma) = \frac{1}{2N\sqrt{\rho\bar{\gamma}_j\gamma}}\left[1-\exp\left(-\frac{\varphi_{\text{AoA},s}^2}{2\sigma_{\text{AoA},s}^2}\right)\right]^2 \left[1-\exp\left(-\frac{\varphi_{\text{AoA},j}^2}{2\sigma_{\text{AoA},j}^2}\right)\right]\frac{\xi_q^2}{A_{0,q}h_{l,q}}\times\frac{\xi_p^2}{A_{0,p}h_{l,p}}\frac{A_{0,j}\xi_j^2}{h_{l,j}}G_{4,5}^{4,2} \left(\frac{A_{0,j}\sqrt{\gamma}}{\partial A_{0,p}A_{0,q}N\sqrt{\rho\bar{\gamma}_j}}\middle|\begin{matrix}-1-\xi_j^2,-2,1+\xi_q^2,1+\xi_p^2\\ \xi_p^2,1,\xi_q^2,1,-2-\xi_j^2\end{matrix}\right). \tag{13}$$

3 Outage probability analysis

The system is in an outage when the channel cannot support the instantaneous information rate. The OP is thus defined as the probability that the instantaneous information rate falls below a threshold rate. In the presence of a jammer, the average OP is expressed as [13]

$$P_o(\bar{\gamma}_j) = \rho\,\Pr\left(\gamma_j \leqslant 1\right). \tag{14}$$

Thus, the average OP can be expressed via its equivalent integral representation:

$$P_o(\bar{\gamma}_j) = \rho\int_0^1 f\gamma_j(\gamma)\mathrm{d}\gamma. \tag{15}$$

By applying the integral property of the Meijer G-function (07.34.21.0084.01) [18] to integrate Eq. (13) over the interval [0, 1], the closed-form expression for the OP is derived as follows:

$$P_o(\bar{\gamma}_j) = \frac{1}{2N\sqrt{\rho\bar{\gamma}_j}}\left[1-\exp\left(-\frac{\varphi_{\text{AoA},s}^2}{2\sigma_{\text{AoA},s}^2}\right)\right]^2\frac{A_{0,j}\xi_j^2}{h_{l,j}}\frac{1}{\pi^{1.5}} \frac{\xi_q^2}{A_{0,q}h_{l,q}}\frac{\xi_p^2}{A_{0,p}h_{l,p}}\times\left[1-\exp\left(-\frac{\varphi_{\text{AoA},j}^2}{2\sigma_{\text{AoA},j}^2}\right)\right] G_{9,11}^{8,5}\left(\left(\frac{A_{0,j}}{2\partial A_{0,p}A_{0,q}N\sqrt{\rho\bar{\gamma}_j}}\right)^2\middle|\begin{matrix}\mathbf{B1}\\ \mathbf{B2}\end{matrix}\right), \tag{16}$$

where

$$\mathbf{B}1=\left\{\frac{1}{2},\frac{-1-\xi_j^2}{2},\frac{-\xi_j^2}{2},-1,-\frac{1}{2},\frac{1+\xi_q^2}{2},\frac{2+\xi_q^2}{2},\frac{1+\xi_p^2}{2},\frac{2+\xi_p^2}{2}\right\},$$

$$\mathbf{B}2=\left\{\frac{\xi_p^2}{2},\frac{1+\xi_p^2}{2},\frac{1}{2},1,\frac{\xi_q^2}{2},\frac{1+\xi_q^2}{2},\frac{1}{2},1,\frac{-2-\xi_j^2}{2},\frac{-1-\xi_j^2}{2},-\frac{1}{2}\right\}.$$

4 Parameter optimization

To further enhance the optical link performance and jamming resilience of the IRS-UAV-assisted FSO system, this section focuses on optimizing the key system and optical parameters, with a rigorous formulation of the bi-objective optimization problem and a tailored low-complexity solution algorithm.

4.1 Problem formulation

Our goal is to enhance the jamming resilience of the IRS-UAV-assisted FSO system while considering the economic cost of deployment. This is formulated as a bi-objective optimization problem, aiming to minimize a weighted sum of the system OP and the total cost.

We formulate a bi-objective optimization problem over the variables N (discrete), P_s, θ_p, φ_p, φ_q, θ_{FOV}, ω_p, and a_p. Since parameters φ_p and φ_q are regulated by the set of phase shifts $\{\psi_s\}$, the optimization of $\{\psi_s\}$ can be characterized by that of parameters φ_p and φ_q.

$$\mathbf{P1}: \min_{N,P_s,\boldsymbol{\theta}_p,\boldsymbol{\varphi}_p,\theta_{\mathrm{FoV}},\omega_p,a_p} \alpha P_o+\beta C_{\mathrm{total}}, \tag{17}$$

s.t.

$C_{\mathrm{total}} \leqslant C_{\mathrm{budget}}$ (total-cost constraint), (17a)

$P_{\min} \leqslant P_s \leqslant P_{\max}$ (transmit-power bound), (17b)

$\mathrm{FoV}_{\min} \leqslant \theta_{\mathrm{FoV}} \leqslant \mathrm{FoV}_{\max}$ (FoV constraint), (17c)

$\theta_{p,\min} \leqslant \theta_p \leqslant \theta_{p,\max}$ (beam-divergence angle bound), (17d)

$\varphi_{p,\min} \leqslant \varphi_p \leqslant \varphi_{p,\max}$ (incident-angle bound at IRS), (17e)

$\varphi_{q,\min} \leqslant \varphi_q \leqslant \varphi_{q,\max}$ (incident-angle bound at D), (17f)

$\omega_p > 0$ (IRS position constraint), (17g)

$a_{p,\min} \leqslant a_p \leqslant a_{p,\max}$ (aperture-size bound), (17h)

$N \geqslant 1,\ N \in \mathbb{N}^+$ (element-count constraint), (17i)

where α and β are non-negative weighting coefficients satisfying $\alpha+\beta=1$, which balance the relative importance of transmission reliability (quantified by $P_o(\bar{\gamma}_j)$) and hardware deployment cost. The selection of α and β can be tailored to practical application scenarios: for high-reliability priority scenarios such as military anti-jamming communications, α can be set close to 1 ($\beta \to 0$) to prioritize outage minimization; for cost-sensitive civilian applications, $\alpha=\beta=0.5$ can be adopted to achieve a balanced trade-off between reliability and cost. The total hardware cost is modeled as $C_{\mathrm{total}} = N \cdot C$, where C is the unit cost of a single IRS element. The constraints ensure that the total cost does not exceed the preset budget C_{budget}, the transmit power, optical angles, and aperture size are within practical hardware limits, and the number of IRS elements is a positive integer.

4.2 Proposed alternating optimization algorithm

Problem (**P1**) is a mixed-integer nonlinear programming (MINLP) problem, which is NP-hard and challenging to solve directly. While AO is a general framework for such problems, its performance depends critically on the variable decomposition strategy and subproblem solver selection, which are often arbitrary in standard AO applications. The core algorithmic contribution of this work is the design of a problem-specific customized AO algorithm tailored to the unique structure of our IRS-UAV-FSO anti-jamming optimization problem, which achieves the theoretical lower bound of computational complexity.

The primary motivations and innovations of our algorithm design are as follows:

(1) Optimal decomposition strategy. Our problem exhibits a specific structure, namely, one discrete variable (N, the number of IRS elements) and seven continuous variables. We adopt a decomposition strategy that first fixes the discrete variable N and optimizes the continuous variables, followed by a re-optimization of N.

(2) The proposed algorithm exhibits a total complexity of $O(K \cdot (T_{\mathrm{PSO}} + N_{\max}))$, where K denotes the number of alternating iterations, T_{PSO} represents the complexity of solving the continuous-variable subproblem via particle swarm optimization (PSO), and $N_{\max}$ is the maximum number of IRS elements (typically $\leqslant 20$ under practical UAV payload constraints). In contrast, a standard AO implementa-

tion for such mixed-integer problems often resorts to a nested architecture, wherein the continuous subproblem is solved independently for each candidate value of N, resulting in a multiplicative complexity of $O(N_{\max} \cdot T_{\mathrm{PSO}})$ per iteration. By decoupling the discrete search from the continuous optimization—exploiting the fact that the continuous subproblem solution is largely insensitive to small variations in N—the proposed scheme reduces the per-iteration cost from multiplicative to additive, thereby achieving linear scaling in the number of IRS elements.

(3) Optimal subproblem solver selection. For the discrete variable N, which has a small feasible domain, we use exhaustive search. This achieves the theoretical lower bound in complexity and guarantees global optimality. For the continuous subproblem, we employ PSO, which is well suited to nonconvex optical parameter optimization. This combination proves significantly more efficient than applying generic solvers to both subproblems, as in standard AO.

The core procedure of the proposed customized AO algorithm is shown in Algorithm 1.

5 Numerical results

This section reports simulation results validating the derived analytical expressions and evaluating the proposed algorithm. We benchmark performance against two classes of baselines, namely, solver-level benchmarks—specifically Genetic Algorithm (GA) and Random Search (RS) as representative meta-heuristic techniques for non-convex problems—and system-level benchmarks, including state-of-the-art anti-jamming IRS-UAV-FSO schemes [13,17] and a non-optimized baseline.

Deep reinforcement learning (DRL) is excluded from this comparison. The proposed method addresses offline parameter optimization under quasi-static FSO conditions with known statistical channel and jamming models. Heuristic search methods thus provide a computationally efficient and appropriate baseline, whereas model-free DRL would impose prohibitive training and deployment costs on resource-constrained UAV platforms without delivering commensurate gains in this setting. Extension to online DRL adaptation for highly dynamic jamming scenarios is left for future study.

The UAV altitude is set to 100 m. For the PSO algorithm, we set the population size to 30, maximum iterations to 50, inertia weight to 0.8, individual learning factor to 1.5, and social learning factor to 2.0. For the GA, we set the population size to 50, maximum generations to 100, crossover probability to 0.8, mutation probability to 0.2, and tournament selection with size 3. For Random Search, we set the number of iterations to 1000 with uniform random sampling from the feasible variable ranges. The default system parameters are summarized in Table 2, aligning with typical FSO communication scenarios and practical UAV-IRS constraints.

Algorithm 1 Alternating optimization for Problem (**P1**)

Initialize: Set iteration index $k = 0$. Initialize continuous variables $\Omega^{(0)} = \{P_s^{(0)}, \theta_p^{(0)}, \varphi_p^{(0)}, \varphi_q^{(0)}, \theta_{\mathrm{FoV}}^{(0)}, \omega_p^{(0)}, a_p^{(0)}\}$ and discrete variable $N^{(0)}$ within their feasible domains.

repeat

$k = k + 1$

Step 1: Optimize continuous variables with fixed N

For fixed $N = N^{(k-1)}$, solve the subproblem for continuous variables:

$$\Omega^{(k)} = \arg\min_{\Omega} \left[\alpha P_o(\Omega, N^{(k-1)}) + \beta C_{\mathrm{total}}(\Omega, N^{(k-1)})\right]$$

s.t. Constraints Eqs. (17a)–(17i).

Using a global optimization algorithm (PSO) to handle non-convexity.

Multiple initial points are recommended to mitigate the risk of poor local minima.

Step 2: Optimize discrete variable N **with fixed continuous variables**

For fixed $\Omega = \Omega^{(k)}$, solve:

$$N^{(k)} = \arg \min_{N \in \{N_{\min}, \ldots, N_{\max}\}} \left[\alpha P_o(\Omega^{(k)}, N) + \beta C_{\mathrm{total}}(\Omega^{(k)}, N)\right]$$

by exhaustive search over the limited integer range.

Calculate the current objective value

$\mathrm{Obj}^{(k)} = \alpha P_o(\Omega^{(k)}, N^{(k)}) + \beta C_{\mathrm{total}}(\Omega^{(k)}, N^{(k)})$

until $\left|\mathrm{Obj}^{(k)} - \mathrm{Obj}^{(k-1)}\right| / \left|\mathrm{Obj}^{(k-1)}\right| \leqslant \eta$ (e.g., $\eta = 10^{-3}$)

Output: Optimized parameters Ω^*, N^*.

Table 2 Default simulation parameters [4,8].

Parameter	Symbol	Value
S-D distance	L_{SD}	1 km
Jamming power	P_j	1 W
Jamming probability	ρ	1.0
Visibility	V	5 km
Receiver FoV angle	θ_{FoV}	6 mrad
AoA fluctuation Std. Dev.	σ_{FoV}	1.2 mrad
Beam divergence angle	θ_p	0.175 mrad
S-IRS incident angle	φ_p	$\pi/4$ rad
IRS-D incident angle	φ_q	0 rad
Aperture radius (S-IRS)	a_p	0.05 m
Aperture radius (IRS-D)	a_q	0.05 m
Jamming distance	L_j	500 m
The distance ratio between S-IRS and IRS-D	w_p	1.0

5.1 Performance analysis results

Figure 3a illustrates the impact of the jamming probability ρ on the system OP. For a fixed average SJR $\bar{\gamma}_j$, the OP increases monotonically with ρ. For instance, at $\bar{\gamma}_j = 10$ dB, increasing ρ from 0.05 to 1.0 degrades the OP by approximately an order of magnitude. However, as $\bar{\gamma}_j$ increases beyond 20 dB, the OP gap between different ρ values diminishes significantly. This indicates that under intermittent jamming, investing in higher legitimate transmit power is more effective for reliability than attempting to precisely estimate or mitigate the jammer's active periods when the average jamming power is moderate.

Figure 3b shows the impact of the IRS position parameter ω_p on the OP. The OP decreases as ω_p decreases, meaning placing the IRS closer to the source node S is beneficial for minimizing the cascaded path loss. This demonstrates that optimizing ω_p is an effective strategy to enhance system robustness.

Figure 4 illustrates OP as a function of the receiver FoV angle θ_{FoV} under malicious jamming with $P_j = 1$ W. As θ_{FoV} increases from 0 to 6 mrad, the OP drops sharply due to improved signal capture capability. Beyond 6 mrad, the OP enters a saturation regime where further expanding the FoV yields diminishing returns. This behavior is attributed to the fixed receiver aperture area ($a_q = 0.05$ m). This saturation behavior indicates that the receiver's ability to collect signal power becomes limited by the aperture size rather than the FoV once the latter exceeds a certain threshold. Moreover, increasing the jamming probability ρ from 0.5 to 1.0 significantly degrades the OP. For instance, at $\theta_{FoV} = 10$ mrad, with $P_s = 0.5$ W and $N = 1$, the OP rises

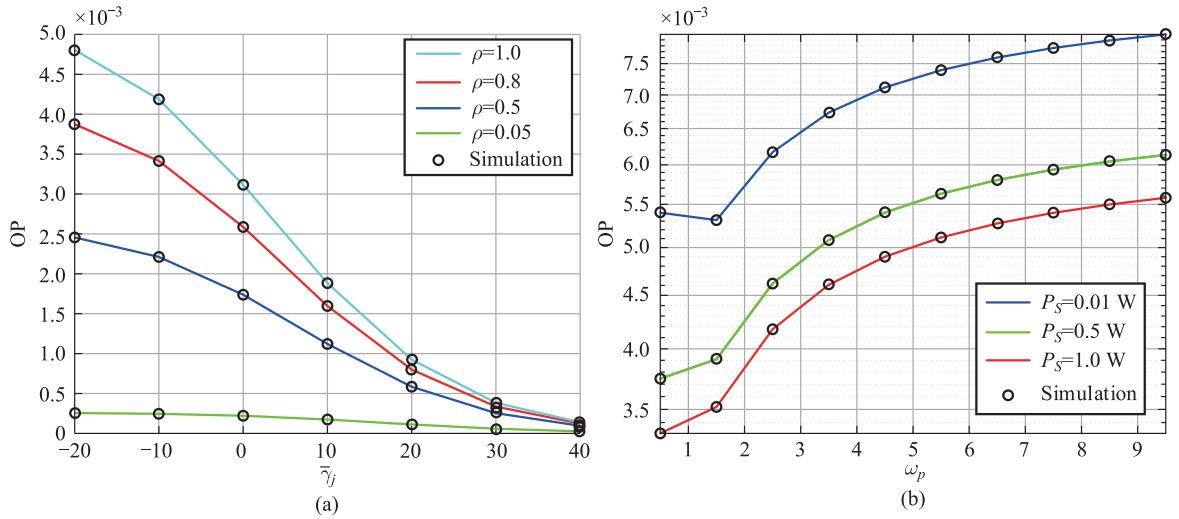

Fig. 3 Impact of key parameters on OP: (a) jamming probability ρ, (b) IRS position parameter ω_p.

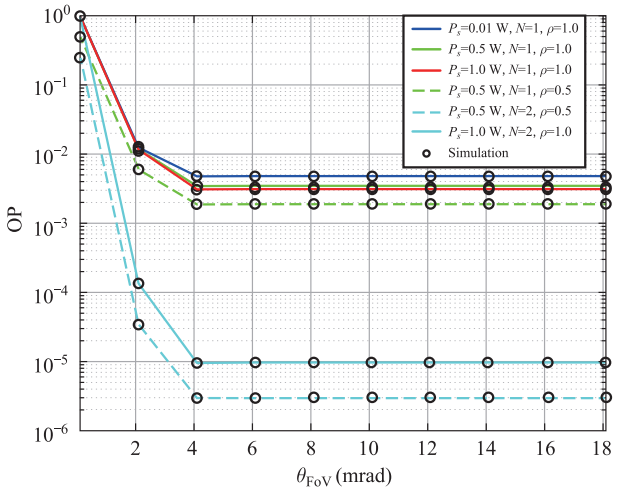

Fig. 4 OP vs. receiver FoV angle under intense jamming.

from 1.9×10^{-3} (at $\rho=0.5$) to 3.5×10^{-3} (at $\rho=1.0$). This notable increase underscores the pronounced vulnerability of the system to the presence of malicious jamming, highlighting that even under identical channel and power conditions, the likelihood of jamming activity directly governs transmission reliability. Furthermore, Fig. 4 also demonstrates that doubling the number of IRS elements from $N=1$ to $N=2$ reduces the OP by more than an order of magnitude. Such a substantial improvement stems from the IRS's ability to achieve coherent combining of reflected signals via intelligent phase control, thereby not only boosting the received signal power but also exploiting spatial diversity. Consequently, the IRS serves as a key enabler for enhancing link robustness against both jamming and fading impairments.

Figure 5 analyzes the joint impact of the aperture sizes a_p (S-IRS link) and a_q (IRS-D link) on the system OP. A non-monotonic relationship is observed for both parameters, where initially enlarging the apertures reduces the OP

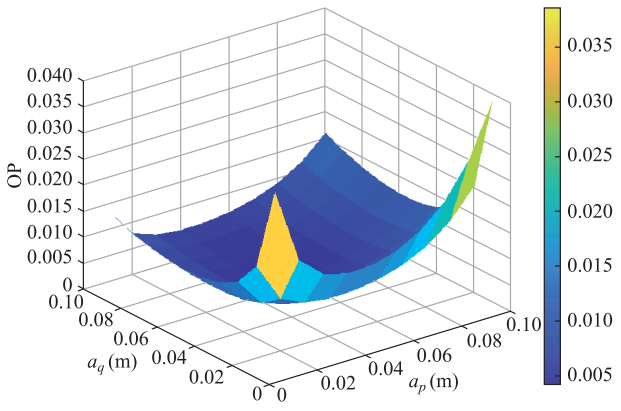

Fig. 5 OP vs. receiver aperture sizes (a_p and a_q).

by capturing more legitimate optical signal power. However, beyond their respective optimal values (approximately 0.05 m for a_p and 0.045 m for a_q under the default simulation settings), further increasing the aperture sizes degrades the OP, as larger apertures collect proportionally more background noise and malicious jamming energy.

To assess local sensitivity around the optimum, we define the sensitivity index as the relative variation in OP induced by a ±10% perturbation of a given parameter from its optimal value. Specifically, a ±10% perturbation of a_q around its optimal value induces a relative OP variation of 22.3% to 28.7%, while an identical perturbation of a_p results in a variation of 17.1% to 20.5%. The resulting sensitivity ratio, defined as the relative impact of a_q versus a_p, falls within the range of approximately 1.3 to 1.4 under the considered nominal operating conditions. This indicates that, within this specific parameter regime, the system exhibits higher sensitivity to the aperture size of the IRS-D link (a_q) than that of the S-IRS link (a_p).

5.2 Parameter optimization results

We now evaluate the performance of the proposed AO algorithm against two benchmarks: GA and RS.

For the reliability-prioritized case ($\alpha=0.99$, $\beta=0.01$, Fig. 6a), the AO algorithm achieves stable convergence within 15 iterations, approximately 2.7× faster than GA (~ 40 iterations). This significant speedup stems from the decomposable structure of the formulated MINLP, where by decoupling the discrete variable (IRS element number N) from continuous variables (transmit power, FoV, aperture sizes), the proposed method avoids the exponential complexity of a joint search over the entire solution space. Specifically, N is optimized via exhaustive search over a small feasible range ($N\in[1,20]$ under practical UAV payload constraints), while the continuous subproblem is solved by PSO with polynomial complexity. By contrast, GA encodes all variables into a single chromosome, incurring redundant crossover and mutation operations that slow convergence. Random Search exhibits large fluctuations in the objective value because each iteration draws independent samples without exploiting historical search information.

For the balanced case ($\alpha=0.5$, $\beta=0.5$, Fig. 6b), where outage reliability and deployment cost are weighted equally, all three algorithms converge to comparable objective values, yet the AO algorithm preserves its speed advantage. This confirms that the decomposition-based framework is robust across different design priorities, accommodating flexible deployment under varying budget and reliability requirements.

To quantify these differences, we compare the final opti-

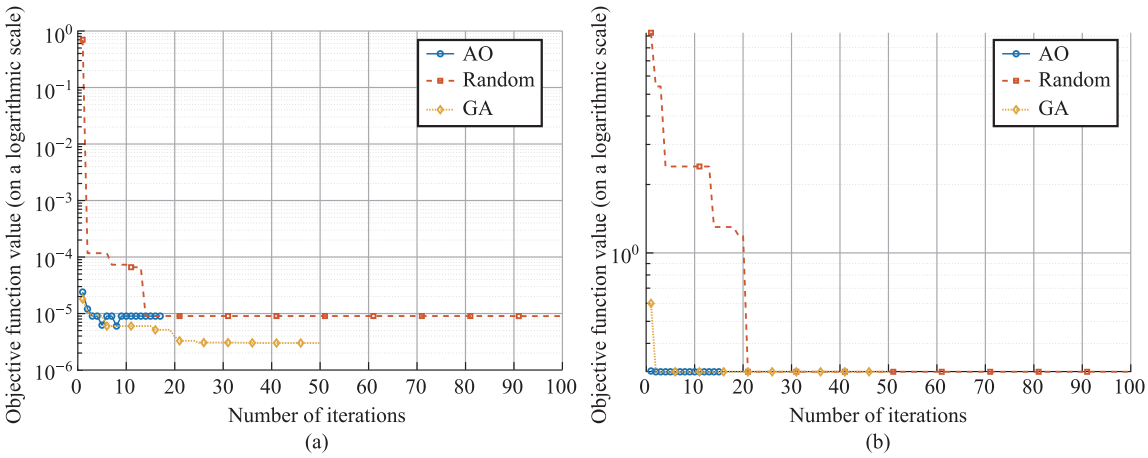

Fig. 6 Comparison of convergence curves of different optimization algorithms: (a) $\alpha = 0.99$, $\beta = 0.01$, (b) $\alpha = 0.5$, $\beta = 0.5$

mized outage probability and computational time. All experiments were performed on an Intel Core i7-12700H CPU with 16 GB RAM, and results were averaged over 50 independent Monte Carlo runs to ensure statistical reliability. The AO algorithm completes optimization in 2.2 seconds, whereas GA and Random Search require 11.8 and 10.0 seconds, respectively. Despite this substantial gap in execution time, the final outage probability achieved by AO deviates from that of GA by less than 8.8%, confirming near-optimal performance with markedly higher efficiency.

From an engineering perspective, the rapid convergence is essential for real-time UAV-assisted FSO systems. Unlike static ground-based IRS deployments, UAV-mounted IRS operates in highly dynamic environments where channel conditions and jamming states vary rapidly. The ability to re-optimize system parameters within tens of iterations enables real-time adaptation to such dynamics, a capability that slower meta-heuristic algorithms such as GA cannot provide.

The results in Table 3a reveal a distinct divergence in optimization strategies under persistent jamming ($\rho = 1.0$). The GA converges to a solution with a notably lower objective value (3.01×10^{-6} versus 9.00×10^{-6}) by aggressively minimizing the transmit power to $P_s = 0.0203$ W. While mathematically optimal for the given weights, such an extremely low power allocation may render the link vulnerable in practice, as it offers little margin against unforeseen channel fluctuations or imperfect channel state information. In contrast, the proposed AO algorithm yields a more balanced configuration with a moderate power reserve ($P_s = 1.498$ W) and standard aperture dimensions, achieving a competitive objective value while maintaining robust operational headroom. This suggests that AO prioritizes engineering practicality alongside mathematical optimization. A consistent pattern across the AO and GA solutions is the selection of only one or two IRS elements. This minimal footprint achieves a favorable performance-cost trade-off and aligns with prior findings that doubling the element count reduces outage probability by over an order of magnitude. When the jamming probability decreases to $\rho = 0.5$ (Table 3b), AO adapts by reducing the transmit power by approximately 53% and adjusting incident angles to mitigate cascaded path loss, while keeping the IRS element count unchanged. This behavior indicates effective adaptability to the dynamic threat environment.

Having examined the optimized parameter configurations, we now turn our attention to the algorithmic conver-

Table 3 Comparison of parameter optimization results of different optimization algorithms: (a) $\rho = 1.0$, (b) $\rho = 0.5$

(a) $\rho = 1.0$	N	P_s(W)	θ_p(rad)	φ_p(rad)	φ_q(rad)	θ_{FoV}(rad)	w_p	a_p(m)
AO	1	1.4980	0.005000	0.5253	0.5233	0.004999	50.00	0.0100
Random	2	0.2001	0.004325	1.0786	0.2750	0.000244	12.68	0.0955
GA	1	0.0203	0.004994	1.2062	1.1766	0.003650	1.47	0.0120
(b) $\rho = 0.5$	N	P_s(W)	θ_p(rad)	φ_p(rad)	φ_q(rad)	θ_{FoV}(rad)	w_p	a_p(m)
AO	1	0.7012	0.004897	1.2217	1.1018	0.004999	49.96	0.0100
Random	3	0.4552	0.002219	1.0122	1.1984	0.001496	0.82	0.0739
GA	2	0.0145	0.004577	1.0461	1.2047	0.000717	2.11	0.0171

gence behavior and the resulting outage performance.

(1) Convergence speed: Fig. 6a compares the convergence behavior of the algorithms. The proposed algorithm converges rapidly within 15 iterations, benefiting from its sequential decomposition of the problem. In contrast, GA requires approximately 40 iterations because of its higher complexity per iteration, and Random Search fails to converge stably even after 50 iterations due to the vast solution space.

(2) Optimized parameters and objective value: Figs. 6a and 7 summarize the optimized parameters and the resulting objective values. The proposed algorithm and Random Search both yield an objective value of 9.00×10^{-6}, whereas GA converges to 3.01×10^{-6}. The GA prioritizes cost reduction and achieves a marginally better objective value by leveraging a larger FoV. However, the proposed algorithm offers a more practically viable trade-off via significantly faster convergence, rendering it suitable for real-time applications in dynamic UAV environments.

(3) Effect of weight selection: Fig. 6b illustrates the convergence behavior when the weights are set to $\alpha=\beta=0.5$, giving equal importance to reliability and cost. All algorithms converge to similar objective values, but the proposed AO algorithm again demonstrates superior convergence speed. This confirms the robustness and efficiency of our optimization framework under different design priorities.

Figure 7 depicts the OP of the proposed AO algorithm and four benchmark schemes (i.e., unoptimized baseline, GA, particle PSO, and gradient descent (GD)) as a function of the average jamming power $\bar{P}_j$, under $\alpha=0.99$ and $\beta=0.01$. It can be observed that the OP of all schemes increases monotonically with $\bar{P}_j$, which is attributed to the aggravated co-channel interference caused by the elevated jamming power in the interference-limited FSO system. The unoptimized scheme yields the worst outage performance, whose OP rapidly approaches 1 even at an extremely low jamming power of 0.5 W, demonstrating the necessity of the proposed optimization design for enhancing system reliability. In contrast, the proposed AO algorithm achieves nearly identical outage performance to the widely adopted GA and PSO meta-heuristic algorithms, and all three schemes significantly outperform the GD-based benchmark over the entire jamming power range. Specifically, at $\bar{P}_j=2$ W, the outage probability of AO, GA, and PSO remains around 0.5, while that of the GD scheme rises to nearly 0.9, which validates the superiority of the proposed AO algorithm in terms of anti-jamming capability and transmission reliability.

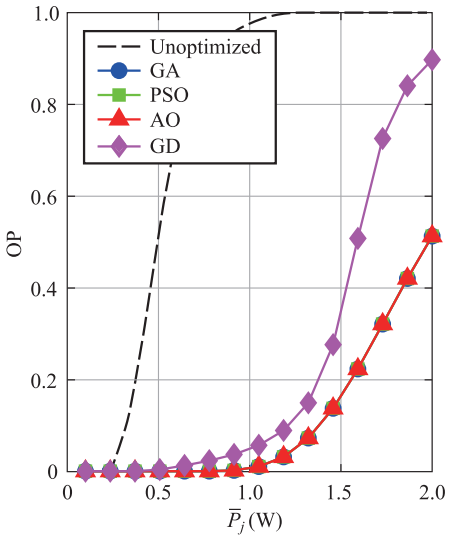

Fig. 7 Outage performance of the proposed AO algorithm versus average jamming power $\bar{P}_j$, compared with unoptimized, GA, PSO and GD benchmarks under system parameters $\alpha=0.99$ and $\beta=0.01$.

To further contextualize the performance of the proposed framework, we compare its outage performance against three representative FSO anti-jamming designs under equivalent hardware constraints. The proposed probabilistic jamming-aware scheme achieves significantly lower outage probability compared to the constant-jamming IRS-UAV-FSO system [13], the IRS element allocation scheme [7], and the non-anti-jamming IRS-FSO baseline [8]. This qualitative advantage, consistent with the quantitative trends observed in Fig. 7, underscores the benefit of explicitly accounting for the intermittent nature of jamming and jointly optimizing the performance–cost trade-off.

6 Conclusion

This paper investigates the outage performance of IRS-UAV-assisted FSO systems subject to probabilistic malicious jamming, with particular emphasis on optical-domain physical impairments that critically affect link reliability. These include saturated AT, PE, AoA fluctuations induced by UAV jitter, and constraints related to receiver optical design. A unified composite channel model incorporating probabilistic jamming is developed, and a novel closed-form expression for the average OP is derived. To balance the trade-off between transmission reliability and hardware deployment cost, a bi-objective optimization problem is formulated, jointly optimizing key optical parameters (beam divergence angle, receiver aperture size, FoV angle) and system parameters (number of IRS elements, transmit power). The resulting MINLP problem is solved using an efficient hybrid AO algorithm, which exploits the natural decomposable structure of the problem to

decouple it into discrete and continuous subproblems for a low-complexity solution. Simulation results validate the accuracy of the analytical derivations and demonstrate that the proposed algorithm converges within 15 iterations, achieving approximately 60% faster convergence than a GA benchmark. Moreover, the optimized design reduces the OP by an order of magnitude compared to non-optimized baselines, while keeping hardware costs within a predefined budget. This work provides a robust and cost-aware design framework for IRS-UAV-enhanced FSO networks and offers practical engineering insights into the optical parameter optimization of anti-jamming FSO systems. Experimental validation of the proposed framework on a hardware testbed represents a valuable direction for future work.

Acknowledgements This research was supported by the National Natural Science Foundation of China (Grant Nos. U21A20511 and 62171478).

Author contribution J.W. carried out the system modeling and theoretical derivations, performed the simulations and optimization algorithm implementation, and drafted the manuscript. D.G. conceived the study, supervised the research, and revised the manuscript critically for important intellectual content. J.L. participated in the validation of analytical expressions and contributed to the simulation design. X.Z. assisted in the channel model analysis and reviewed the manuscript. D.D. participated in the data curation and helped with the performance comparison. All authors read and approved the final manuscript.

Declarations

Competing interests The authors declare that they have no competing interests.

Availability of data and materials The data that support the findings of this study are available from the corresponding author, upon reasonable request.

References

1. Ning, Z., Li, T., Wu, Y., Wang, X., Wu, Q., Yu, F.R., Guo, S.: 6G communication new paradigm: the integration of unmanned aerial vehicles and intelligent reflecting surfaces. IEEE Commun. Surv. Tutor **27**(6), 3382 (2025)
2. Ishida, T., Naila, C.B., Okada, H., Katayama, M.: Performance analysis of IRS-assisted multi-link FSO system under pointing errors. IEEE Photonics J **16**(4), 1–10 (2024)
3. Zhang, Z., Chen, W., Wu, Q., Li, Z., Zhu, X., Chen, J., Cheng, N.: Multiple intelligent reflecting surfaces collaborative wireless localization system. IEEE Trans. Wirel. Commun **24**(1), 134–148 (2025)
4. Gu, L., Mohajer, A.: Joint throughput maximization, interference cancellation, and power efficiency for multi-IRS-empowered UAV communications. Signal Image Video Process **18**(5), 4029–4043 (2024)
5. Dai, M., Huang, N., Wu, Y., Gao, J., Su, Z.: Unmanned-aerial-vehicle-assisted wireless networks: advancements, challenges, and solutions. IEEE Internet of Things Journal **10**(5), 4117–4147 (2023)
6. Paul, P., Bhatnagar, M.R.: Jamming threats in free-space optics. IEEE Communications Magazine **60**(12), 104–108 (2022)
7. Singh, P., Salameh, H.B., Bohara, V.A., Srivastava, A., Ayyash, M.: Jamming-resilient mirror element allocation scheme for OIRS-aided UAV-based FSO networks. IEEE Trans. Intell. Veh. 1–12 (2024)
8. Chen, B., Zhu, X.: Outage-guaranteed transmission for IRS-assisted FSO systems. Opt. Express **32**(14), 25420 (2024)
9. Sipani, J., Sharda, P., Bhatnagar, M.R.: IRS-assisted UAV based FSO system: modeling approach for hovering UAV. In: Proceedings of 2024 IEEE 100th Vehicular Technology Conference (VTC2024-Fall), pp. 1–5 (2024)
10. Vishwakarma, N., R, S., Diamantoulakis, P.D., Karagiannidis, G.K.: Cascaded FSO systems with optical reflecting surfaces. IEEE Internet Things J **11**(23), 38631–38644 (2024)
11. Xu, G., Zhang, N., Xu, M., Xu, Z., Zhang, Q., Song, Z.: Outage probability and average BER of UAV-assisted dual-hop FSO communication with amplify-and-forward relaying. IEEE Trans. Vehicular Technol **72**(7), 8287–8302 (2023)
12. Qu, L., Xu, G., Zeng, Z., Zhang, N., Zhang, Q.: UAV-assisted RF/FSO relay system for space-air-ground integrated network: a performance analysis. IEEE Trans. Wirel. Commun **21**(8), 6211–6225 (2022)
13. Saxena, P., Chung, Y.H.: Analysis of jamming effects in IRS assisted UAV dual-hop FSO communication systems. IEEE Trans. Vehicular Technol **72**(7), 8956–8971 (2023)
14. Sharma, P., Swaminathan, R.: Performance analysis of UAV-based IRS-assisted FSO communication systems. In: Proceedings of 2025 IEEE 101st Vehicular Technology Conference (VTC2025-Spring), pp. 1–6 (2025)
15. Wang, J., Gao, D., Ding, H., Dong, J., Zhang, X., Li, J.: Performance analysis of IRS-assisted multi-link FSO system under UAV-enabled jamming. In: Proceedings of ICC 2025 - IEEE International Conference on Communications, pp. 3125–3131 (2025)
16. Wang, J., Gao, D., Chen, R., Zhang, X.: Impact of UAV-assisted jamming on IRS-enhanced FSO systems: a Gamma-Gamma turbulence and pointing error perspective. Opt. Express **33**(19), 40774–40800 (2025)
17. Singh, P., Bany Salameh, H., Bohara, V.A., Srivastava, A., Ayyash, M.: On mitigating reactive jamming with dynamic resource allocation in optical IRS and UAV-assisted FSO-based networks. Phys. Commun **67**, 102520 (2024)
18. MeijerG. Available at the website of functions.wolfram.com/PDF/MeijerG.pdf. Wolfram Research (2020)

Jingyu Wang received the M.S. degree from the College of Information and Communication, National University of Defense Technology in 2013. He is currently pursuing the Ph.D. degree in optical engineering at Huazhong University of Science and Technology. His main research interest is optical wireless communication.

Dingshan Gao received the Ph.D. degree from the Institute of Semiconductors, Chinese Academy of Sciences in 2004. After that, he served as a post-doctoral researcher at Huazhong University of Science and Technology. Currently, he is a professor at Huazhong University of Science and Technology/Wuhan National Laboratory for Optoelectronics. He is currently the Chinese leader of the Sino-French "PHOTONET" joint research network. His research interests include silicon-based photonics, optical communications, nano-photonics, and integrated quantum optics. He has published more than 50 peer-reviewed papers in international authoritative journals such as *Optica*, *Physical Review Letters*, *Science Reports*, *Optics Letters*, and *Optics Express*. He is the associate editor of the international *IET Optoelectronics* journal.

Juan Li received the Ph.D. degree from Air Force Engineering University. She is currently a lecturer at the Engineering University of the Information Support Force. Her research interests focus on wireless communication systems, including channel modeling, performance analysis, and advanced transmission techniques. She has published more than 10 SCI journal papers in related fields.

Xinliang Zhang received the Ph.D. degree from the Huazhong University of Science and Technology (HUST) in 2001. He is currently a Professor with the Wuhan National Laboratory for Optoelectronics and the Former Dean of School of Optical and Electronic Information, HUST. He has published 200 related papers in international journals or conferences proceedings. His current research interests include all-optical signal processing, optical communications, and silicon photonics.

Deqiang Ding received the Ph.D. degree from Xi'an University of Technology. He is now a professor and Master's supervisor at the Engineering University of the Information Support Force. His research interests lie in wireless optical communications, including FSO systems, turbulence mitigation, and link performance optimization.